

Effects of Dehydration on the Viscoelastic Properties of Vocal Folds in Large Deformations

Amir K. Miri, François Barthelat, and Luc Mongeau, *Montreal, Canada*

Summary: Dehydration may alter vocal fold viscoelastic properties, thereby hampering phonation. The effects of water loss induced by an osmotic pressure potential on vocal fold tissue viscoelastic properties were investigated. Porcine vocal folds were dehydrated by immersion in a hypertonic solution, and quasi-static and low-frequency dynamic traction tests were performed for elongations of up to 50%. Digital image correlation was used to determine local strains from surface deformations. The elastic modulus and the loss factor were then determined for normal and dehydrated tissues. An eight-chain hyperelastic model was used to describe the observed nonlinear stress-stretch behavior. Contrary to the expectations, the mass history indicated that the tissue absorbed water during cyclic extension when submerged in a hypertonic solution. During loading history, the elastic modulus was increased for dehydrated tissues as a function of strain. The response of dehydrated tissues was much less affected when the load was released. This observation suggests that hydration should be considered in micromechanical models of the vocal folds. The internal hysteresis, which is often linked to phonation effort, increased significantly with water loss. The effects of dehydration on the viscoelastic properties of vocal fold tissue were quantified in a systematic way. A better understanding of the role of hydration on the mechanical properties of vocal fold tissue may help to establish objective dehydration and phonotrauma criteria.

Key Words: Vocal fold–Dehydration–Mechanical stiffness–Loss factor–Digital image correlation–Eight-chain model.

INTRODUCTION

Voice production involves the self-sustained, flow-induced oscillations of the vocal folds. They are a layered structure of ligament, muscle, and soft tissue located within the larynx. Voice quality strongly depends on the viscoelastic properties of the vibrating mucosal tissue. The mechanical deformations of the vocal folds under load, as for many soft biological tissues, are governed at the microscopic level by interactions between the extracellular matrix proteins and the interstitial fluid. Frequent rehydration, supplied from the vocalis muscle and the epithelium, is required to maintain regular phonatory function. Local or systemic dehydration may lead to disordered vocalization.¹ For example, maintaining adequate tension in the vocal fold is difficult in dehydrated vocal folds, particularly at high pitches.¹ Dehydration may occur at the surface from convective mass transport or within the body from osmotic transport through the ligament.²

During phonation, the vocal folds are elongated by cricoarytenoid muscle contraction. A transverse mucosal wave is observed to propagate on the vocal folds surface, involving deformations of the multilayered lamina propria. The high-frequency vibrations of the lamina propria in the sagittal plane are small in amplitude relative to large-amplitude, quasi-static oscillations in the transverse plane. The hydration level is believed to significantly affect the stiffness and the viscosity of the vocal fold lamina propria (as stated below), and water mass transports are believed to occur over timescales that are

much larger than the oscillation period. Therefore, the role of hydration on the viscoelastic properties of the vocal folds must be better understood to model their phonatory function.

The phonation threshold pressure (PTP) is defined as the minimum air pressure needed to initiate and maintain vocal fold self-oscillations. This metric has been used as an objective index to evaluate the effects of dehydration on voice quality. Finkelhor et al³ investigated the relationship between the PTP and the viscoelastic properties of vocal fold tissue. The PTP was measured using excised larynges submerged in three saline solutions of low, medium, and high sodium chloride concentrations. It was inferred that the mucosal viscosity decreased as the water content was increased. The influence of hydration level on voice quality was investigated by Verdolini-Marston et al¹ using human subjects. The oral pressure for dry, hydrated, and untreated larynges was measured during voiceless stop consonants at low, medium, and high pitches. The greatest oral pressure, as an estimate of PTP, was observed for dry conditions and high pitches.

The mechanical stiffness of excised vocal folds was measured using indentation in the coronal plane at locations on the superficial layer.⁴ Dry mucosa was found to be stiffer than hydrated tissues. In another study,⁵ phonatory effort was estimated through various physiological and psychological observations to investigate the inverse relation between hydration level and PTP. Jiang et al⁶ showed that the surface rehydration of the vocal folds reduces the PTP as well as the minimum air-flow required to sustain phonation. Hemler et al⁷ studied the effects of the humidity of airflow over the surface of dissected human vocal folds. They observed increases in viscosity and stiffness following exposure to dry air, even when the tissue was systemically rehydrated from the ligament. The effects of dehydration and rehydration on the vocal linear viscoelastic properties were studied using shear rheometry at low frequencies, that is, below 15 Hz.² Canine mucosal tissue samples

Accepted for publication September 15, 2011.

From the Biomechanics Laboratory, Department of Mechanical Engineering, McGill University, Montreal, QC, Canada.

Address correspondence and reprint requests to Luc Mongeau, Biomechanics Laboratory, Department of Mechanical Engineering, McGill University, 817 Sherbrooke Street West, Montreal, QC H3A 2K6, Canada. E-mail: luc.mongeau@mcgill.ca

Journal of Voice, Vol. 26, No. 6, pp. 688-697

0892-1997/\$36.00

© 2012 The Voice Foundation

doi:10.1016/j.jvoice.2011.09.003

were sequentially incubated in isotonic, hypertonic, and hypotonic solutions. Four- to seven-fold increases in stiffness and a frequency-dependent increase in viscosity were observed in dehydrated vocal folds.

Sivasankar *et al*⁸ showed that dehydration through inhaled dry air or impairments in surface hydration is detrimental to phonation. The barrier functions of dehydrated vocal fold epithelia were estimated by recording the changes in their epithelial resistance, paracellular pathway morphology, and protein integrity.⁹ Witt *et al*¹⁰ also investigated the increase in phonation threshold flow rate following exposure to dry air. The correlation between the degree of surface dehydration and the phonation threshold flow (PTF) rate was quantitatively estimated in an *ex vivo* canine larynx model. An increase of 50–100% was observed in the PTF of vocal folds exposed to dry airflow. Hanson *et al*¹¹ attempted to evaluate the physiological impact of dehydration by examining the recoverability of vocal folds, that is, the capacity for water absorption up to the initial level. Their analysis was based on a biphasic model of the fluid-solid structure interactions.¹¹ The rate of convective water transport in vocal folds was estimated during speech production using numerical simulations.¹² A computational model was introduced to quantify the mass loss during inhalation. There is no model available for comparable studies of systemic water transport rates at the present time. The present study may help to fill this gap.

The purpose of the present study was to better quantify the relationship between the level of hydration and the viscoelastic properties of the vocal fold lamina propria through traction tests for strains up to 50%. Body dehydration was induced through immersion of the tissue in a hypertonic buffer solution. This procedure is believed to reduce the water content through changes in osmotic pressure. Porcine vocal fold tissue was used. Dissected vocal fold tissue samples were subjected to alternating mechanical traction tests and dehydration. The local strain on the tissue surface was measured using digital image correlation (DIC) during tensile tests for the accurate estimation of the viscoelastic properties.¹³

The loading response was found to vary linearly with the axial stretch strains smaller than 15%, as shown later. At higher strains than 15%, the relationship between the applied force and the resulting elongation was nonlinear with a stiffening trend. Phenomenological models of the equilibrium stress-strain response of soft tissues were used in the past to interpret this type of result,¹⁴ but these models do not yield any insights into possible structure-property relationships. In this work, the experimental data were modeled using a microstructure-based model. The porcine vocal fold lamina propria has a composition similar to that of humans,^{15,16} and it has a similar mechanical structure composed of elastin and collagen. As a result, its mechanical behavior is also comparable with that seen in humans.¹⁷ The three-dimensional organization of elastin and collagen in a similar tissue was imaged by Miri *et al*¹⁸ using multiphoton microscopy. To link the structure and macroscopic properties, the eight-chain model of Arruda and Boyce¹⁹ was used. This statistically based model has been successfully applied in the past to soft tissues such as skin.²⁰ Hypothesizing structural similarities between

the fibrous network of skin and that of vocal folds,¹⁸ the eight-chain model was used to model the measured viscoelastic response. The model parameters were adjusted based on the response of the tissue to uniaxial tension forces. The results yield a possible interpretation of the basic physics of the material response on a microscopic scale, which may be useful in multiphase mechanical models of the vocal fold tissue (eg, Zhang *et al*²¹).

METHODS

Sample preparation

Healthy porcine larynges ($m = 10$) were obtained from a local abattoir immediately postmortem. They were immersed in a 0.9% saline solution and transported to the laboratory for testing. Within a few hours, the sample dissection was initiated by removing connective soft tissues around the larynx. A midsagittal cut was made in the anterior section. Two hemilarynges were separated in a way that the thyroid cartilage was preserved at the anterior commissure (Figure 1A). Following the removal of the ventricular (ie, superior¹⁷) vocal folds using a small scalpel, the true (ie, inferior¹⁷) vocal folds were then separated from the subglottal wall (Figure 1A). Small portions of the arytenoid and thyroid cartilages, with 5–8 mm width and 3–5 mm thickness, were kept to facilitate gripping of the vocal folds during axial tension tests (Figure 1B). The vocalis muscle was smoothly excised from the vocal fold lamina propria. Care was taken not to damage the lamina propria to ensure loading uniformity. A portion of the muscle was left in the neighborhood of ending cartilages, as shown in Figure 1B. The dissection of all samples was done within 3–4 hours postmortem.

Test protocols

A three-step traction test procedure was used as follows. Traction tests were performed using an EnduraTEC tester (Electro-Force ELF 3200; Bose Inc., Eden Prairie, MN), equipped with a digital camera (Flea2; Point Grey Research Inc., Richmond, BC) to capture the surface deformation. The second-axis output signal of the ELF machine, used in simple uniaxial mode, was used to trigger the camera to synchronize displacement, force, and images. A schematic of the test apparatus is shown in Figure 2. The apparatus was set in a displacement-control mode. The displacement actuator range was 12 mm. The applied displacement was also compensated using a proportional, integral and derivative (PID) controller.

The thickness of the samples was measured at four different locations using a caliper (Mitutoyo, Tokyo, Japan) with a precision of 1 μm . A speckle pattern was applied onto the surface, as described in the following subsection. The sample was installed between two grips via four black silk (3.0 metric) sutures on each end (Figure 1B and 2A). Because the current method uses noncontact optical measurements, the results are not affected by the sutures. The parts attached to the tissue only transmit the extension loading. The sample was submerged in a normal phosphate buffer saline (PBS) at $37^\circ\text{C} \pm 0.5^\circ\text{C}$ such that a thin layer of fluid covered the epithelium. A fiber optic

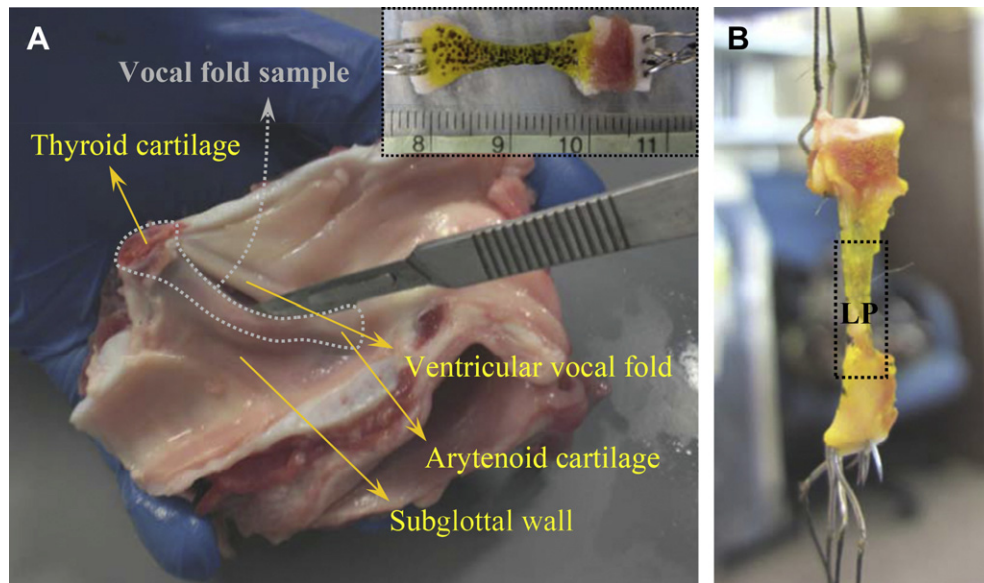


FIGURE 1. A. Porcine hemilarynx and a vocal fold sample prepared for mechanical tensile test. B. Vocal fold LP. LP, lamina propria.

light source (Cole-Parmer Instrument Co., Montreal, QC, Canada) was also used to illuminate the sample (Figure 2).

The dehydration protocol was applied as follows. While submerged in PBS, the sample was subjected to a quasi-static cyclic ramp loading at a rate of 0.1 mm/s followed by a 1-Hz sinusoidal loading. The solution was then replaced. The tissue was kept in a (30% NaCl) hypertonic solution over a period of 30 minutes. The temperature was held constant at $37^{\circ}\text{C} \pm 0.5^{\circ}\text{C}$. A similar loading history was then applied with the sample immersed in the same hypertonic solution for a second round of traction tests. One last round was carried out following a 30-minute submersion in the same hypertonic solution. The three-round procedure was then performed on another set of samples bathed in the normal solution (PBS) to supply baseline data (ie, normal protocol).

Digital image correlation

Surface deflections were quantified using DIC to determine the local strain field.²² Tissue dyes (Thermo Fisher Scientific, Ontario, ON, Canada) were used to create a random speckle pattern on the surface of the tissue. A bright dye was applied to produce a uniform background and then the black dye was applied randomly (Figure 1A). The tissue sample was submerged in the solution with the superior surface of the sample near the fluid surface to minimize optical distortion. The commercially available software package *Vic-Snap* (Correlated Solutions Inc., Columbia, SC) was used for the kinematic analysis of the recorded images. The displacement field was obtained from analysis of deformed and undeformed images. The strain field was then calculated using a finite difference approximation of the displacement gradients.

The DIC procedures are as follows. One reference image of the nominal undeformed body is chosen over the area of interest. The randomized speckle pattern over the area creates a unique grayscale distribution over the region analyzed. Since

multiple pixels may have the same grayscale values, a subset of pixels with a predetermined size is chosen and the intensity distribution within that region is calculated. The images are divided into equal subsets, with each subset identified by a unique pattern. The speckle pattern should be random. The size of the speckle dots must be smaller than that of the chosen subsets. The motion of any specific point between two pixels affects the average intensities of both the pixels. Neither has the same value as in the previous image. An interpolation field is then created. A computer algorithm is used to estimate the grayscale values of points between pixels. The subsequent position of each subset is obtained from the best correlation in the surrounding subsets.

Constitutive model

A constitutive law expresses the relation between stress components and the strain field. The so-called eight-chain model was originally proposed to describe mechanical behavior from the entropy changes of long-chain elements in polymers.¹⁹ This model has been found to be accurate in modeling the mechanical extension of soft tissues.²⁰ The formulation of this hyperelastic model may be based on the strain energy potential W . For the case of incompressible material, the eight-chain model has the following form of strain energy potential²⁰

$$W = n k_B \theta \sqrt{N} (\lambda_c \beta - \sqrt{N} \ln[\sinh(\beta)/\beta]) \quad (1)$$

where $k_B = 1.3807 \times 10^{-23}$ Nm/K is Boltzman's constant, and $\theta = 310$ K represents the absolute temperature. $\ln(\bullet)$ is the natural logarithm and $\sinh(\bullet)$ is the hyperbolic sinusoidal function. The term β is defined as

$$\beta = L^{-1}(\lambda_c/\sqrt{N}) \quad (2)$$

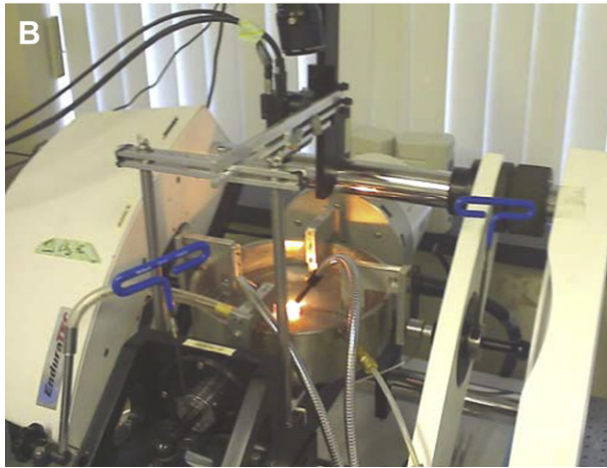
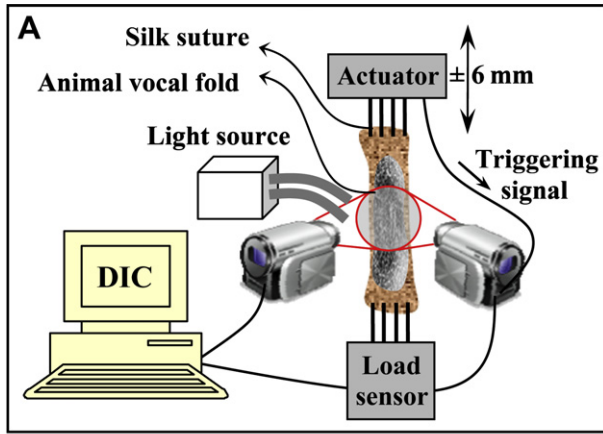


FIGURE 2. A. Schematic of the experimental apparatus for mechanical tensile test (two cameras are shown for the case of three-dimensional imaging). B. Picture of the apparatus for axial testing of porcine vocal folds. One camera was used for imaging the planar deformation field. Note that the tissue sample was submerged in the normal solution (PBS) for the first round and in the hypertonic solution (30% NaCl) during the second and third rounds. PBS, phosphate-buffered saline; DIC, digital image correlation.

where λ_c is the chain stretch, that is,

$$\lambda_c = (\lambda_1^2 + \lambda_2^2 + \lambda_3^2)^{1/2} / \sqrt{3} \quad (3)$$

and $L^{-1}(\bullet)$ is the inverse Langevin function.¹⁹ λ_i 's ($i = 1, 2, 3$) represent the material stretches along the global coordinates, that is, longitudinal, transverse, and thickness directions. The material parameters are N , which is the number of rigid links of a specific length, and n , which is the network molecular chain density. Hence, high/low N and n values imply, respectively, long/short and strong/weak collagen fibrils. From Equation 1, the true stress-stretch relation for the case of axial tension experiment may be expressed in terms of two unknown parameters, N and n , as:

$$\sigma_1 = \frac{n k_B \theta \sqrt{N}}{3} L^{-1} \left(\frac{\lambda_1^2 + 2/\lambda_1^2}{\sqrt{N}} \right) \frac{\lambda_1^2 - 1/\lambda_1}{\lambda_1^2 + 2/\lambda_1} \quad (4)$$

For more details on this formulation, the reader is referred to Bischoff et al.²⁰ From the axial force F obtained from the ELF machine and the longitudinal stretch $\lambda_1 (\equiv 1 + \epsilon)$, calculated by DIC, the following force-stretch relation is deduced

$$F = \frac{1}{3} h w n k_B \theta \sqrt{N} L^{-1} \left(\frac{\lambda_1^2 + 2/\lambda_1^2}{\sqrt{N}} \right) \frac{\lambda_1 - 1/\lambda_1}{\lambda_1^2 + 2/\lambda_1} \quad (5)$$

where h and w denote, respectively, the effective thickness and width of each sample (Figure 2). The optimal combination of these parameters was established based on a least-square error regression procedure. All experimental data were parameterized using Equation 5. The root square of the mean squared error was between 0.04 and 0.12 for most of the cases.

RESULTS AND DISCUSSIONS

Mass history

The loss of interstitial fluid induced by osmotic pressure potential was presumed to cause no variation in the molecular composition of the matrix protein.² Between initial and final weights of those samples that were subjected to the dehydration protocol, no significant difference was observed. Hence, another two sets of porcine vocal folds ($m = 4$) were subjected to both protocols for the estimation of water loss. The cartilage at the anterior and posterior ends significantly contributed to the overall weight. To eliminate possible bias from the cartilage, the arytenoid and thyroid cartilages were extracted during the sample preparation. A central area of approximately 15×4 mm (the dash-dot region in Figure 1B) was preserved. Weighing was performed before and after each round of the traction test experiments. The samples were weighed using an electronic balance (Thermo Fisher Scientific, Ontario, ON, Canada). The overall results, normalized with the initial weight $M = 0.2416 \pm 0.0292$ g for hypertonic protocol and $M = 0.1974 \pm 0.0657$ g for normal protocol, are shown in Figure 3. On extension, the tissue appears to have absorbed water in the first round of traction tests. A notable mass loss ($\Delta M = 0.0562 \pm 0.0032$ g from step "2" to step "3") occurred during the first 30-minute submersion in the hypertonic solution. Contrary to what was expected, the tissue then absorbed water during the two rounds of traction tests.

A hypothetical justification for the dehydration (from step 2 to step 3 in Figure 3) and the mechanical extension (from step 3 to step 4 in Figure 3) is illustrated in Figure 4, based on postulated biophysical mechanisms that were originally proposed for articular cartilages. Concentration here refers to the abundance of solute particles (like chloride sodium molecules) per volume of the solution. Arbitrary constants were introduced for better understanding of the sketch. The osmotic pressure is basically the pressure difference across a permeable interface separating two solutions of different concentrations. At time $t = 0$ (step 2 of Figure 3), the osmotic pressure forces the water out of the tissue at a high flow rate. The hydrostatic pressure, force exerted by the fluid molecules on an immersed body, at this point in time should be identical on both sides of the interface because the tissue was kept in a buffer solution before submersion. After

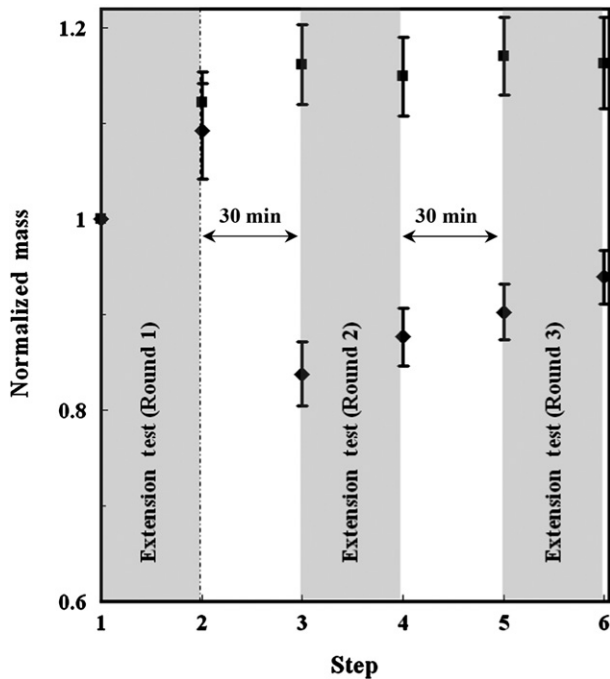


FIGURE 3. Normalized mass history of porcine vocal folds for two different protocols: normal solution ■ ($m = 4$) and hypertonic solution ◆ ($m = 4$). (Note: the time period for the extension tests was approximately 20 minutes).

a short time, at $t = t_1$, a large hydrostatic pressure gradient is formed across the interface. Water may then be expelled from the tissue with a significantly reduced flow rate. After a certain time, at $t = t_2$, equilibrium is reached between the osmotic and hydrostatic pressures. Thus, the rate of water transport into and out of the tissue should be equal.

At a later time at $t = t_3$ (step 3 of Figure 3), the tissue is extended along the axial direction. The hydrostatic pressure inside the tissue is increased because of global force equilibrium. Solute particles such as chloride sodium migrate into the tissue because the membrane is penetrable. This denaturalizes and reverses the osmotic pressure potential. The new potential is stronger than the hydrostatic pressure compared with the case of the normal solution. When the tensile force is removed, at $t = t_4$, equilibrium is reached across the interface. The state of equilibrium has changed since some particles have migrated into the tissue. The final water content (step 4 of Figure 3) is thus larger than that of the equilibrium condition before loading (step 3 of Figure 3). Further studies are needed to confirm this proposed hypothetical mechanism.

A typical plot of the axial force recorded by the load cell versus the displacement out of the tensile test machine arm is shown in Figure 5. In this experiment, the peak displacement value was 11 mm. Force (or stress) relaxation is observed because the force magnitude for a given displacement decreases between successive cycles. Hysteresis loops are observed over each period. The hysteretic area and the elastic constant are both significantly larger in the first cycle than in the subsequent cycles. Such a trend is also observed in the case of engineering rubber materials, for example. A few initial cycles are

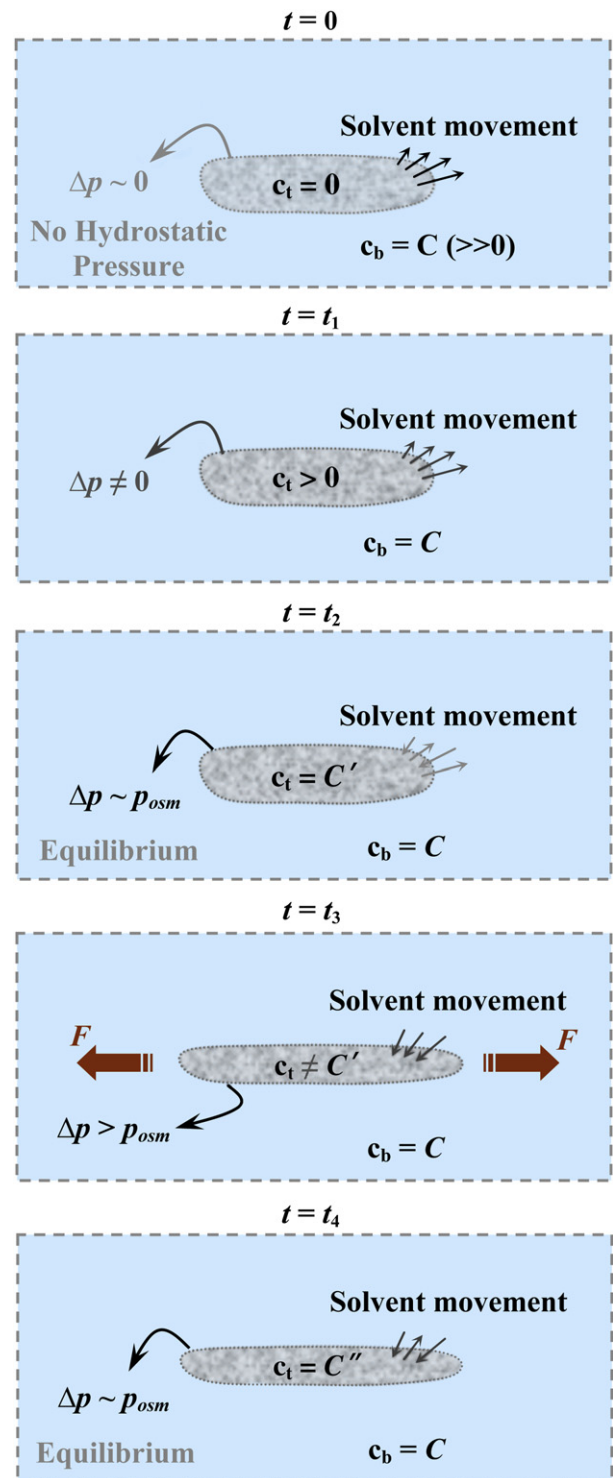


FIGURE 4. Postulated mechanisms of water loss/absorption in the tissue submerged in the hypertonic solution (ie, 30% NaCl) and subjected to mechanical test at time t ($0 < t_1 < t_2 < t_3 < t_4$). Parameters c_t and c_b denote the solute concentrations of the tissue and bath, respectively. C , C' , C'' are real-valued constants. The symbols p and p_{osm} indicate hydrostatic and osmotic pressures, respectively.

often applied to precondition the tissue (eg, Alipour et al¹⁷) to avoid subsequent relaxation. This procedure may cause the loss of possibly valuable information because the relaxation

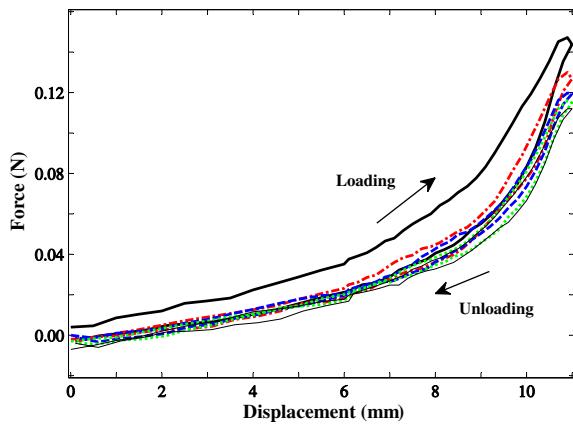


FIGURE 5. Traction force versus arm displacement for five successive load cycles of ramp displacement at 0.1 mm/s. (— 1st cycle; - - - 2nd cycle; - - - 3rd cycle; ···· 4th cycle; — 5th cycle).

process may reveal interesting details of the microstructure of the material. In contrast with rubber, however, a similar but less pronounced strain softening relaxation was observed in the second and third rounds of the tension tests. The hierarchical organization of the tissue may change during submersion, which may change the entropy. Or the water change may have contributed changes in tissue viscoelasticity because the solid network already absorbed water during submersion. It has been reported that tissue hydration reduces viscosity.¹⁰ Nevertheless, a significant hysteresis area is observed in the first three cycles. Hence, entropy variations may have possibly contributed more than water content. Beyond the third cycle, the mechanical response appears to reach a steady state and consequently water content should be, on average, constant.

Strain field

Optical measurements based on DIC were made to evaluate the planar strain field. The mechanical tester provides in-plane Green's strain tensor through the optical tracking of four dots (four corners of a square). Silicon rubber samples were subjected to axial traction tests using both the four-dot optical measurement and DIC. Reasonable agreement was observed for the axial strain values. Generally, the strain obtained from the displacement of the arm (Figure 2) is not accurate because of local deformations at the tissue-suture connections and the inhomogeneity of the strain field. This was verified through comparisons between the strain-displacement correlations of a physical rubber model and porcine vocal folds. At large strains, significant differences were observed. Optimal parameters such as the aperture and exposure time of the camera were obtained by trial and errors in preliminary studies.

In-plane strain components were calculated using Vic-2D (Correlated Solutions Inc., Colombia, SC). A subset size of 25×25 pixels was selected over the area of interest, which includes almost the entire surface of the vocal fold. For large elongations, the software analyzed each image by tracking the points in previous images. The data near the boundaries was ignored because of the edge effects. Areas that were out of focus caused significant errors. A circular area with a 3-mm diameter

was thus selected to calculate the average axial strain magnitude. This process was followed to ensure consistency across samples.

The strain distributions of one sample are shown in Figure 7. The reference image shows the initial state. A pre-stress of less than 10% of the maximum stress was applied to uncurl the undeformed tissue. Contours of axial strain, shown in Figure 6, illustrate the inhomogeneity of the strain field and, consequently, of the mechanical stress during deformation. In the area of interest, the axial strain ranges from 21.8% to 28.9% for image 1 and from 37.6% to 64.4% for image 2. The strain reaches a local maximum value along a line that connects two sutures. A region of significant shear strain was observed, which violates the assumption of pure axial strain normally made in uniaxial tension tests. This emphasizes the importance of local strain measurements for the accurate determination of the axial strain. Area averaging over the selected region may be used to filter shear strain variations as needed.

The strain history in successive cycles was investigated. For a quasi-static loading, the strain values were consistently repetitive. For dynamic sinusoidal loading, however, the strain increased slightly over successive cycles. Averaged peak values for the fourth and fifth cycles of each round are reported. During the second and third rounds, while the samples were submerged in a hypertonic solution, the strain magnitude did not vanish completely when the displacement was zero. This residual stress may be related to water loss in the vocal fold tissue (Figure 3), which may have shrunk the tissue and consequently increased the stress contribution in the extracellular matrix because of a reduction in the tissue cross section.

Effects of dehydration on vocal fold stiffness and viscosity

Overall stresses, calculated using Equation 4, versus strain values for all cases are shown in Figure 7 and 8. The associated model parameters that were used to generate the figures are reported in Table 1. Low-amplitude shear strains associated with the linear viscoelastic properties of dehydrated vocal folds were reported by Chan and Tayama.² These data were compared with the initial shear modulus, μ_0 , calculated using the eight-chain model in the present study and the results are shown in Table 1. A nearly four-fold increase in shear modulus with dehydration was observed, which is consistent with the lower range of the data of Chan and Tayama.² The average Young's modulus of six porcine vocal folds, with standard deviation, was reported¹⁷ to be 16.3 ± 2.9 kPa, a much lower magnitude than obtained in the present study (40.5 ± 15.7 kPa from 10 samples). The discrepancy may be attributed to the fact that strain estimates based on arm displacement, as opposed to optical-based local strain measurements, tend to cause an underestimation of Young's modulus.¹³

The tangent modulus, that is, the slope of the stress-strain curve, is a measure of mechanical stiffness. For large strains, it was greatly increased in dehydrated tissues. The free-length parameter of the fibers, N , decreased with dehydration. This suggests a shortening of the effective length of the collagen fibers. When the liquid is expelled from the tissue and the salt molecules are drawn in, the fibers may become more

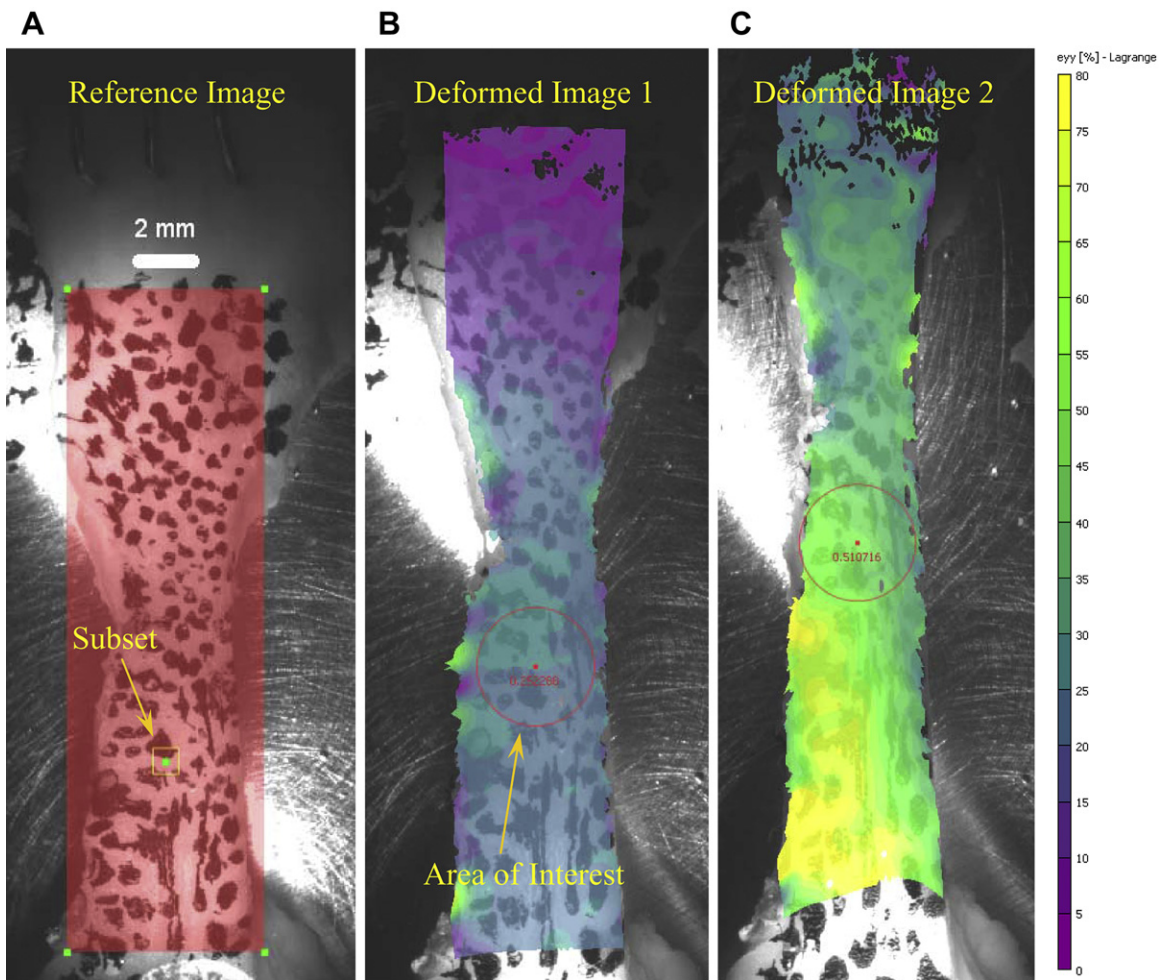


FIGURE 6. Reference image and two subsequent deformed images with superimposed axial strain contours of one vocal fold sample subjected to the ramp loading (0.1 mm/s). **A.** Reference image. **B.** Deformed image for 5-mm extension. **C.** Deformed image for 11-mm extension.

entangled. This may create additional physical (and possibly chemical) cross-links between the fibers. The accompanying rise in the network-density parameter of the fibers, n , suggests a denser distribution of protein networks. This is consistent

with the reduction of volume expected following water loss. A comparison between the second round and the third round reveals that dehydrated tissue may not tolerate additional modification, even if the water content is different. The

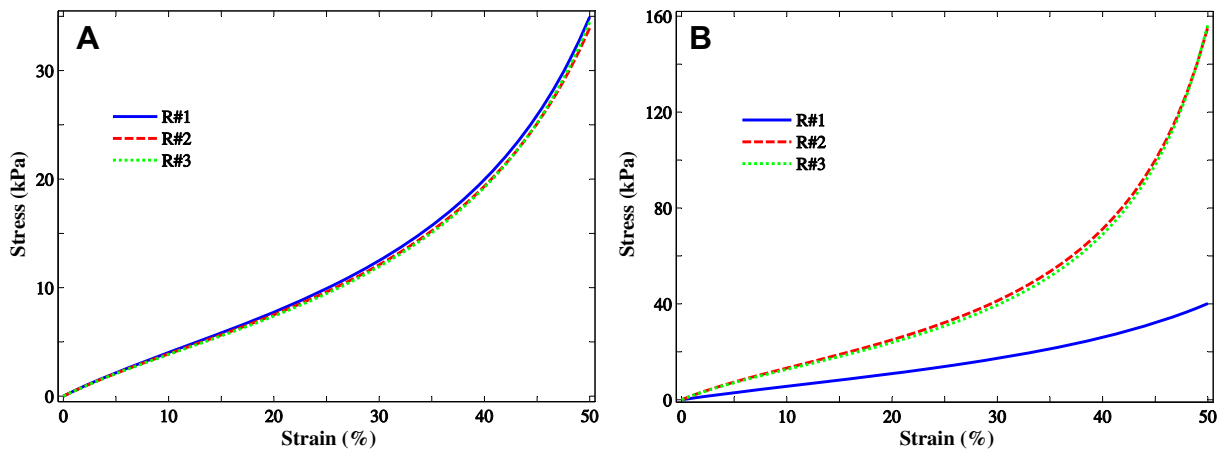


FIGURE 7. **A.** Axial stress versus axial strain of porcine vocal folds ($m = 5$) subjected to quasi-static loading in the normal solution. (— round 1; - - - round 2; ····· round 3). **B.** Axial stress versus axial strain of porcine vocal folds ($m = 5$) subjected to quasi-static loading in the hypertonic solution. (— round 1; - - - round 2; ····· round 3).

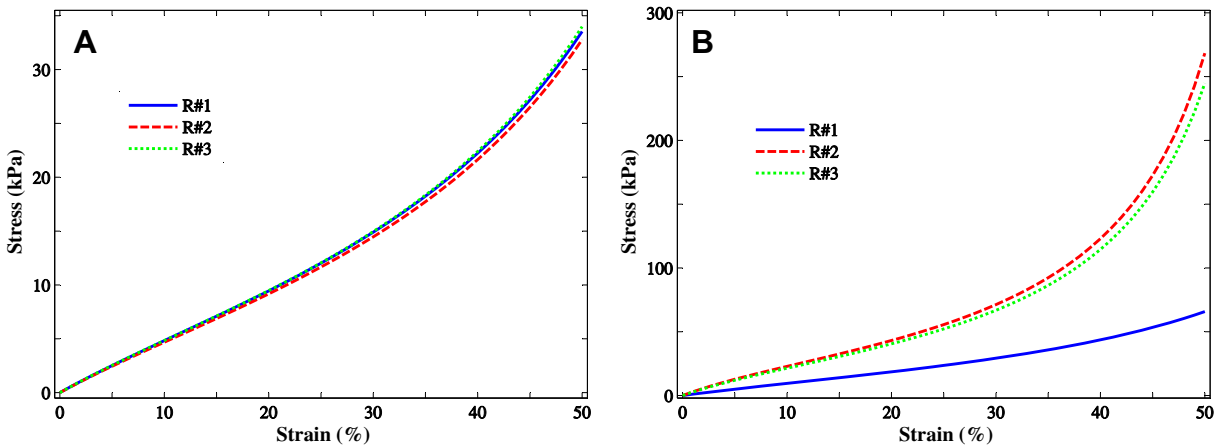


FIGURE 8. A. Axial stress versus axial strain of porcine vocal folds ($m = 5$) subjected to dynamic loading (1 Hz) in the normal solution. (— round 1; - - - round 2; ····· round 3). B. Axial stress versus axial strain of porcine vocal folds ($m = 5$) subjected to dynamic loading (1 Hz) in the hypertonic solution. (— round 1; - - - round 2; ····· round 3).

irreversibility² of the dehydration process was observed in the current protocol.

The nonlinear trend of the stress-strain curves, shown for different rounds in Figures 7 and 8, are the same for various strain levels. The tangent modulus, or the stiffness, for dynamic loading is higher than that for quasi-static loading. As seen above, higher stiffness is a result of water removal. It can be concluded that the water plays less of a role for dynamic loading than for quasi-static loading. This may explain in part the need for hydration following continuous and long high-pitch phonation,⁵ when the vocal folds are extended over a long time period. Another factor is of course surface dehydration. The data are amenable to interpretation in light of mixture theories to model the vocal fold tissue under nonlinear loading (eg, Hanson et al¹¹). The data reported here may be useful as a baseline for model verifications.

Most previous studies have focused on the effects of dehydration on tissue viscosity, particularly at the level of the superficial layer (eg, Witt et al¹⁰). Although vocal folds may undergo surface dehydration for *in situ* tests, body dehydration, used in the present study, yields information that may be a better representation of the bulk behavior of the tissue. Note that average

data for stretching releasing (loading-unloading) were not reported because the maximum stretches were different for various samples. This was because of the tests being performed in a displacement-control mode. The complete data are reported in Table 2. To calculate the mechanical loss factor ζ , stretching and releasing curves were fitted with a polynomial of degree 5, and then the loop integral (ie, the dissipated energy) was divided by the area under the stretching curve (ie, the extension energy).

The loss factor, ζ , is inversely correlated with the propensity for self-sustained oscillations. Phonation normally occurs when mechanical energy losses within the vocal fold lamina propria are small. The loss factor in dehydrated tissue samples is greater than 30%. In contrast, the loss factor of hydrated tissue was found to be smaller than 10%. Thus, a 20% decrease in water mass, estimated from the data of Figure 3 and the tissue porosity of 80%, led to a five-to-seven-fold increase in loss factor. Similar stress-strain curves were observed for the five dehydrated samples. The load-releasing history in dehydrated tissues is very similar to that of the normal tissues. It may be concluded that dehydration mainly affects the stretching response of the vocal fold tissue, when it is longitudinal, and extracellular water may not contribute to the resistance of the tissue during load release.

TABLE 1. Eight-chain Model Parameters and Initial Shear Modulus for Two Different Protocols: Normal Solution ($m = 5$) and Hypertonic Solution ($m = 5$)

Normal Solution					Hypertonic Solution				
Load	R	N	$n (1/m^3) \times 10^{-23}$	μ_0 (kPa)	Load	R	N	$n (1/m^3) \times 10^{-23}$	μ_0 (kPa)
Quasi-static	1	1.18 ± 0.07	8.48 ± 1.77	17.4 ± 5.83	Quasi-static	1	1.28 ± 0.03	14.2 ± 7.88	18.2 ± 9.98
	2	1.18 ± 0.08	8.19 ± 2.02	17.4 ± 5.87		2	1.12 ± 0.04	21.6 ± 10.3	60.3 ± 29.6
	3	1.17 ± 0.07	7.81 ± 2.88	16.7 ± 6.42		3	1.12 ± 0.03	20.1 ± 8.49	58.7 ± 25.7
Dynamic (1 Hz)	1	1.31 ± 0.26	14.6 ± 6.55	23.8 ± 14.4	Dynamic (1 Hz)	1	1.31 ± 0.12	23.3 ± 15.7	25.7 ± 13.6
	2	1.30 ± 0.25	13.4 ± 7.11	22.8 ± 15.3		2	1.10 ± 0.06	37.3 ± 25.7	99.3 ± 49.2
	3	1.30 ± 0.27	13.8 ± 7.32	24.7 ± 17.9		3	1.10 ± 0.07	36.6 ± 27.3	96.5 ± 51.9

R#i stand for the i^{th} round of traction test.

TABLE 2.
Energy Loss Magnitudes of Porcine Vocal Folds for Two Different Protocols: Normal Solution (m = 5) and Hypertonic Solution (m = 5)

Normal Solution					Hypertonic Solution				
Sample	$\epsilon_{\max}(\%)$	Energy Loss (ζ)			Sample	$\epsilon_{\max}(\%)$	Energy Loss (ζ)		
		R#1	R#2	R#3			R#1	R#2	R#3
1	47.9	0.064	0.047	0.041	1	58.5	0.059	0.414	0.401
2	66.8	0.096	0.101	0.099	2	62.8	0.075	0.387	0.378
3	45.9	0.027	0.022	0.013	3	67.9	0.091	0.571	0.545
4	48.8	0.054	0.058	0.043	4	60.3	0.065	0.293	0.283
5	52.6	0.057	0.067	0.076	5	44.1	0.056	0.401	0.392

R#i stand for the i^{th} round of traction test.

The parameter ϵ_{\max} is the upper limit for the average axial strain in the tissue.

The contribution of the fluid phase must be accounted for to properly model the viscoelastic response of vocal fold tissue. Any accurate model should capture the releasing response of the tissue when the factors associated with water are removed. The stretching response must be matched with the results for 20% water loss, for example, five-to-seven-fold increase of ζ at high strains. Considering the stretch-dependent viscosity as a function of tissue porosity would be one possible way to capture such trends in mathematical models. Hence, the results of this study may provide a framework for the modeling of the viscoelastic response of the vocal folds for large deformations.

CONCLUSIONS

The viscoelastic response of dehydrated vocal fold tissues for large extensions was investigated. A uniaxial tension test setup, equipped with a digital camera, was used to impose quasi-static and dynamic cyclical mechanical loading on porcine vocal folds, whereas a hypertonic solution was used to expel water from the tissue. A record of the mass history revealed significant mass changes during loading. The tissue was found to absorb water when initially submerged in a hypertonic solution and subjected to mechanical extension. The tangent modulus of the dehydrated tissue was significantly increased relative to that of the hydrated tissue and varied with the strain magnitude. The eight-chain model previously used in statistical mechanics was used to interpret stress-strain results based on the free length and the network density of the fibers. In addition, large hysteresis areas for dehydrated tissues indicated a rise in internal viscosity, reaching values of 50% in some cases. This may substantiate the reported increase in phonation effort with dehydration. This study may be useful for the clinical assessment of body dehydration.

Acknowledgments

This work was supported by NIDCD grant R01-DC005788 from the National Institute of Deafness and Other Communication Disorders (National Institutes of Health). The authors would like to express their gratitude to Professor Rosaire Mongrain (Montreal Heart Institute Research Centre, Montreal, QC,

Canada) and Professor Thomas Quinn (Chemical Engineering Department, McGill University, Montreal, QC, Canada) for sharing their facilities.

REFERENCES

- Verdolini-Marston K, Titze IR, Druker DG. Changes in phonation threshold pressure with induced conditions of hydration. *J Voice*. 1990;4:142–151.
- Chan RW, Tayama N. Biochemical effects of hydration in vocal fold tissues. *Otolaryngol Head Neck Surg*. 2002;126:528–537.
- Finkelhor BK, Titze IR, Durham PL. The effect of viscosity changes in the vocal folds on the range of oscillation. *J Voice*. 1988;1:320–325.
- Haji T, Mori K, Omori K. Experimental studies on the viscoelasticity of the vocal fold. *Acta Otolaryngol*. 1992;112:151–159.
- Verdolini K, Titze IR. Dependence of phonatory effort on hydration level. *J Speech Hear Res*. 1994;37:1001–1007.
- Jiang JJ, Ng J, Hanson D. The effects of rehydration on phonation in excised canine larynges. *J Voice*. 1999;13:51–59.
- Hemler RJB, Wieneke GH, Lebacqz J, Dejonckere PH. Laryngeal mucosa elasticity and viscosity in high and low relative air humidity. *Eur Arch Otorhinolaryngol*. 2001;258:125–129.
- Sivasankar M, Erickson E, Schneider S, Hawes A. Phonatory effects of airway dehydration: preliminary evidence for impaired compensation to oral breathing in individuals with a history of vocal fatigue. *J Speech Lang Hear Res*. 2008;51:1494–1506.
- Sivasankar M, Erickson E, Rosenblatt M, Branski RC. Hypertonic challenge to porcine vocal folds: Effects on epithelial barrier function. *Otolaryngol Head Neck Surg*. 2010;142:79–84.
- Witt RE, Regner MF, Tao C, Rieves A, Zhuang P, Jiang JJ. The effect of dehydration on phonation threshold flow in excised canine larynges. *Ann Otol Rhinol Laryngol*. 2009;118:154–159.
- Hanson KP, Zhang Y, Jiang JJ. Ex vivo canine vocal fold lamina propria rehydration after varying dehydration levels. *J Voice*. 2011;25:657–662.
- Wang S. Simulation and analysis of water transport from the human larynx during speech production. M.Sc. dissertation, McGill University, QC; 2009.
- Kelleher JE, Zhang K, Siegmund T, Chan RW. Spatially varying properties of the vocal ligament contribute to its eigenfrequency response. *J Mech Behav Biomed Mater*. 2010;3:600–609.
- Min YB, Titze IR, Alipour F. Stress-strain response of the human vocal ligament. *Ann Otol Rhinol Laryngol*. 1995;104:563–569.
- Hahn MS, Kobler JB, Starcher BC, Zeitels SM, Langer R. Quantitative and comparative studies of the vocal folds extracellular Matrix; I: elastic fibers and hyaluronic acid. *Ann Otol Rhinol Laryngol*. 2006a;115:156–164.

16. Hahn MS, Kobler JB, Zeitels SM, Langer R. Quantitative and comparative studies of the vocal folds extracellular Matrix; II: collagen. *Ann Otol Rhinol Laryngol.* 2006b;115:225–232.
17. Alipour F, Jaiswal S, Vigmostad S. Vocal fold elasticity in the pig, sheep, and cow larynges. *J Voice.* 2011;25:130–136.
18. Miri AK, Tripathy E, Mongeau L, Wiseman, PW. Nonlinear Laser Scanning Microscopy of Human Vocal Folds. *The Laryngoscope.* 2012;122:356–363.
19. Arruda EM, Boyce MC. A three-dimensional constitutive model for the large stretch behavior of rubber elastic materials. *J. Mech Phys Solids.* 1993;41:389–412.
20. Bischoff JE, Arruda EM, Grosh K. Finite element modeling of human skin using an isotropic, nonlinear elastic constitutive model. *J Biomech.* 2000; 33:645–652.
21. Zhang Y, Czerwonka L, Tao C, Jiang JJ. A biphasic theory for the viscoelastic behaviors of vocal fold lamina propria in stress relaxation. *J Acoust Soc Am.* 2008;123:1627–1636.
22. Spencer M, Siegmund T, Mongeau L. Determination of superior surface strains and stresses, and vocal fold contact pressure in a synthetic larynx model using digital image correlation. *J Acoust Soc Am.* 2008;123: 1089–1103.